LAWRENCE
LIVERMORE
NATIONAL
LABORATORY

LLNL-TR-793762

Composite 4YSZ-Al2O3 Nanofibers Prepared by Electrospinning and Thermal Processing

M. S. Ross, J. P. Kelly, L. R. Finkenauer, J. J. Haslam

October 14, 2019

Disclaimer

This work performed under the auspices of the U.S. Department of Energy by Lawrence Livermore National Laboratory under Contract DE-AC52-07NA27344.

Composite 4YSZ-Al_2O_3 Nanofibers Prepared by Electrospinning and Thermal Processing

M. S. Ross,[1, a)] J. P. Kelly,[1, b)] L. R. Finkenauer,[1, c)] and J. J. Haslam,[1, d)]

[1]Polymer and Ceramics Group, Materials Engineering Division, Lawrence Livermore National Laboratory, 7000 East Avenue, Livermore, California, 94550

[a)]ross59@llnl.gov, [b)]kelly70@llnl.gov, [c)]finkenauer1@llnl.gov, [d)]haslam2@llnl.gov

Abstract: The relationship between solution properties and processing parameters for novel yttria-alumina-zirconia nanofibers electrospun in a constant electric field is explored through systematic variation of precursor content and aging of the polymer gel. The upper solution viscosity and conductivity limit for electrospinning with an electric field strength of 0.84 kV/cm were ~1000 cP and ~5 mS/cm, respectively. There is a predictive relationship between volumetric flow rate and solution viscosity, conductivity, and surface tension; however, there is not a strong relationship between as-spun fiber diameters, ranging between 100 and 300 nm, and any solution property. The gelation mechanism by which aqueous polyvinylpyrollidone (PVP), zirconium acetate, and aluminum/yttrium nitrate solutions age is speculated to arise from zirconium acetate hydrolysis and polymerization, facilitating intermolecular hydrogen bonding between zirconium acetate complexes, PVP functional groups, and disassociated ionic species. The 4YSZ-Al_2O_3 ceramic nanofiber diameters ranged between 50 and 100 nm depending on the volume percent of the ceramic phases. The annealed fibers appear amorphous and without excessive grain coarsening, indicating that a heat treatment of 1000°C for 2 hours is sufficient to produce tough, refractory nanofibrous membranes relevant for high-temperature filtration applications.

INTRODUCTION

Non-woven polymeric and inorganic nanofiber membranes are being explored for applications such as tissue engineering,[1, 2] catalytic substrates,[3, 4] and filtration[5, 6] due to their excellent mechanical properties, increased surface areas, and high permeabilities. Nanofibers can be produced through template synthesis,[7] self-assembly,[8] and electrospinning,[9] among other techniques. Electrospinning is the most widely used nanofiber manufacturing process, relying on an electric field formed between a biased emitter and collector to eject, stretch, and whip a solvent-polymer-precursor solution into nanofibers. Electrostatic repulsion within the solution overcomes the surface tension of a droplet formed at the emitter, while solution viscosity prevents the formation of separate droplets as material is ejected. The solution traverses towards the collector, allowing the solvent to evaporate and the fiber to solidify before depositing (**Figure 1**). Precursor spinnability and nanofiber morphology are dependent on solution properties like conductivity (σ), surface tension (γ), and viscosity (η), as well as electrospinning parameters like applied voltage, emitter-to-collector distance, emitter diameter, and solution feed rate.[10, 11, 12, 13]

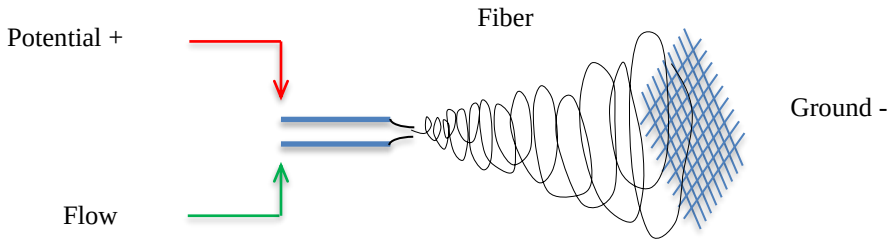

FIGURE 1: Typical electrospinning experimental setup.

Electrospinning precursor solutions may include additional salts to precipitate ceramic nanofibers upon subsequent thermal processing. Zirconia (ZrO_2) and alumina (Al_2O_3) are widely used engineering ceramics due to their thermal stability, chemical inertness, and mechanical properties. Further strengthening is obtained by minimizing grain sizes[14] and critical flaw sizes in the microstructure by reducing fiber diameters in the case of fibrous ceramics.[15] Extrinsic toughening, such as transformation toughening, is obtained in ZrO_2 by engineering the microstructure so that it contains a dispersion of metastable particles that transform and expand when a crack tries to propagate through the microstructure (**Figure 2**).[16, 17] The diffusionless martensitic transformation and expansion of the metastable tetragonal phase to the monoclinic phase compresses the crack tip to inhibit crack propagation and promotes multiple microcracks to form instead of allowing a single crack to propagate catastrophically.[18, 19, 20, 21] Transformation toughening is achieved by substituting lower-valent oxide additives, commonly yttria (Y_2O_3) or magnesia (MgO), into the zirconia fluorite crystal structure and conscious thermal processing for mixtures of zirconia phases.

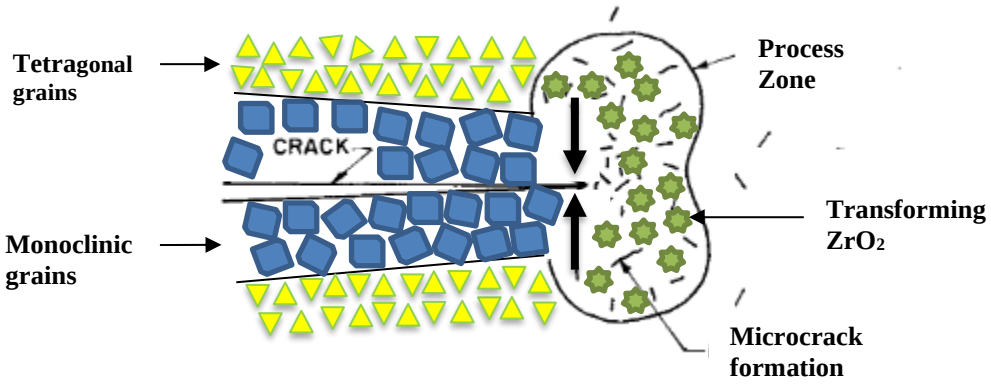

FIGURE 2: The stress induced by a propagating crack tip induces the diffusionless transformation of small metastable zirconia grains to large stable grains, compressing the macrocrack, promoting microcracking, and toughening the microstructure.

Alumina is a strong, refractory ceramic, but generally has a lower bulk fracture toughness than toughened ZrO_2 (e.g., 5 MPa/m$^{1/2}$ compared to 6.5 MPa/m$^{1/2}$).[17] Alumina toughening is achieved by addition of zirconia or stabilized zirconia and is known as zirconia toughened alumina (ZTA), with fracture toughness values from 5 to 13 MPa/m$^{1/2}$ depending on the agglomerate size,[17, 18, 19, 22] volume fraction,[17, 23] and phase composition[24, 25, 26] of zirconia in the microstructure. Conversely, the addition of alumina in a stabilized zirconia matrix suppresses grain growth during sintering,[27] improving strength and fracture toughness. Alumina toughened zirconia (ATZ) reduces zirconia crystal structure instability and sintering activity at higher temperatures.[28] There are mechanical and thermal benefits for compositing alumina with stabilized zirconia across all compositions. Alumina and zirconia composite nanofibers have been electrospun[29,30]; however, electrospinning of alumina and yttria-stabilized zirconia (YSZ) composite nanofibers has not currently been reported in literature. This is a communication of the electrospinning and characterization of electrospun yttria-alumina-zirconia nanofibers across various composite compositions.

EXPERIMENTAL PROCEDURES

All precursor solutions were prepared with zirconium acetate (~16 wt% Zr, Sigma Aldrich, St. Louis, MO) solution in acetic acid and yttrium nitrate hexahydrate ($Y(NO_3)_3 \cdot 6H_2O$, Sigma Aldrich, St. Louis, MO) in a 96Zr:8Y molar ratio to oxidize a solid solution phase with 4mol% Y_2O_3 relative to ZrO_2, known as 4YSZ. To investigate the spinnability of the alumina-yttria-stabilized zirconia system, an array of solutions with variable volume percent of the ceramic phases were produced. The initial, 100% volume 4YSZ solution was synthesized to produce 0.32 cm^3 of 4YSZ; this value was multiplied by the desired volume fraction and density of 4YSZ (ρ ~ 6.075 g/cm^3) to determine the amount of added zirconium acetate and yttrium nitrate hexahydrate. The remaining volume was multiplied by the density of α-Al_2O_3 (ρ ~ 3.95 g/cm^3) and converted to a mass of aluminum nitrate nonahydrate ($Al(NO_3)_3 \cdot 9H_2O$,

Alfa Aesar, Ward Hill, MA). The precursors were added to a 1:1 by weight water and ethanol solution with 8.6 wt% polyvinylpyrrolidone (PVP, average molecular weight Mw ~ 1,300,000, Alfa Aesar, Ward Hill, MA) relative to the solvents. The solutions were left to magnetically stir for 72 hours before being characterized and electrospun. The solutions and their precursor compositions are listed in **Table I** and labeled by the 4YSZ volume fraction:

Table I: Precursor solution concentrations

4YSZ vol%	ZrA wt%	$Y(NO_3)_3 \cdot 6H_2O$ wt%	$Al(NO_3)_3 \cdot 9H_2O$ wt%
100	8.242	0.473	0
90	7.414	0.426	0.917
80	6.587	0.378	1.834
50	4.111	0.236	4.576
20	1.642	0.094	7.311

The solutions were characterized twice a week for 4 weeks using a rotational rheometer (Brookfield DV3T, CP-52 spindle, Middleboro, MA), a conductivity probe (Mettler Toledo FP30, Columbus, OH), and a surface tensiometer (Kibron AquaPi, Helsinki, Finland). Electrospinning was performed on a Fluidnatek LE-10 electrospinner (Bioinicia, Paterna, Valencia, Spain) with an attached iDS UI-1220LE camera to monitor jet morphology (**Figure 3**). A constant electric field strength of approximately 0.84 kV/cm was chosen based on the jet stability of the 80vol% 4YSZ-Al_2O_3 solution. The emitter and collector, separated by 17.25 cm, were biased at 9.5 kV and -5 kV, respectively. The solution was pumped from a syringe, through a capillary tube, to a 0.025-inch inner diameter, single nozzle needle at optimal feed rates to minimize dripping frequency. Optimal feed rates were found by first overfeeding the solution, and then backing off the solution flow to an underfed condition, establishing a range of viable feed rates. The feed rate at which the solution droplet growth was stabilized by jet ejection for the longest time was considered the optimal feed rate. The collector was a mylar covered drum which rotated clockwise at 600 RPM. Additional ambient parameters, such as temperature and humidity, were also recorded.

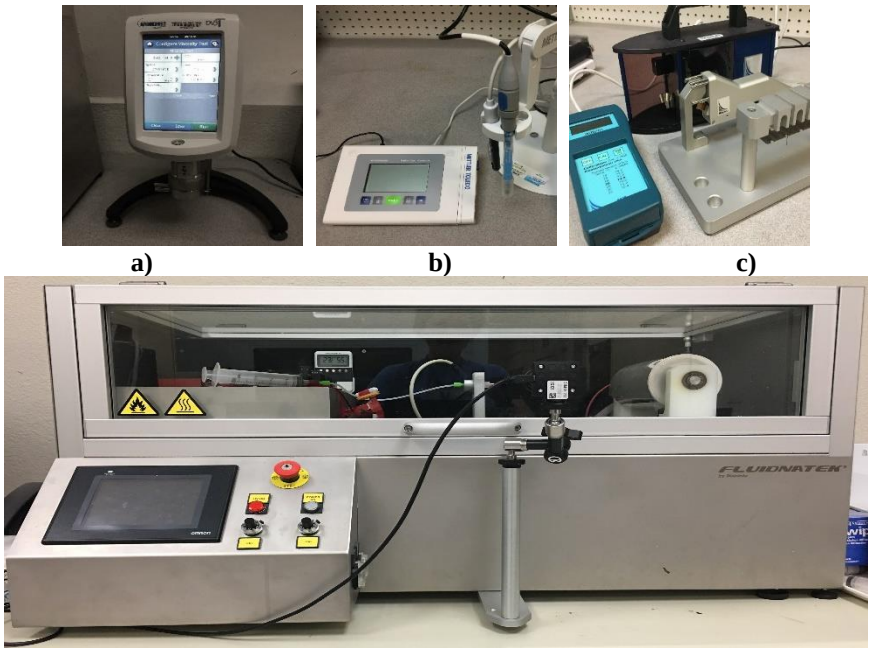

FIGURE 3: Equipment used to characterize solution a) viscosity, b) conductivity, and c) surface tension for d) electrospinning.

The as-spun nanofibers were then peeled from the mylar backing and annealed at 1000°C for 2 hours with heating and cooling rates of 5°C/min. Scanning electron microscopy (SEM) and energy dispersive X-ray analysis (EDX) performed on a Phenom Pro Desktop SEM (Thermo Fisher Scientific, Waltham, MA) was used in conjunction with image processing with ImageJ[31] to measure fiber diameters and to determine their compositions.

RESULTS

Initial zero-shear solution viscosity and surface tension is mainly influenced by precursor, polymer, and solvent concentration.[12] Each solution had an initial viscosity within 500 to 700 centipoise range and an initial surface tension between 33 and 36 mN/m depending on the concentration of zirconium acetate. Solution conductivity increased with the introduction of $Al(NO_3)_3$ as the ionic strength, or concentration of free ions in solution, increased. When using acetate and nitrate precursors, the PVP solution aged with time, evident by increasing viscosity and surface tension (**Figure 4**).

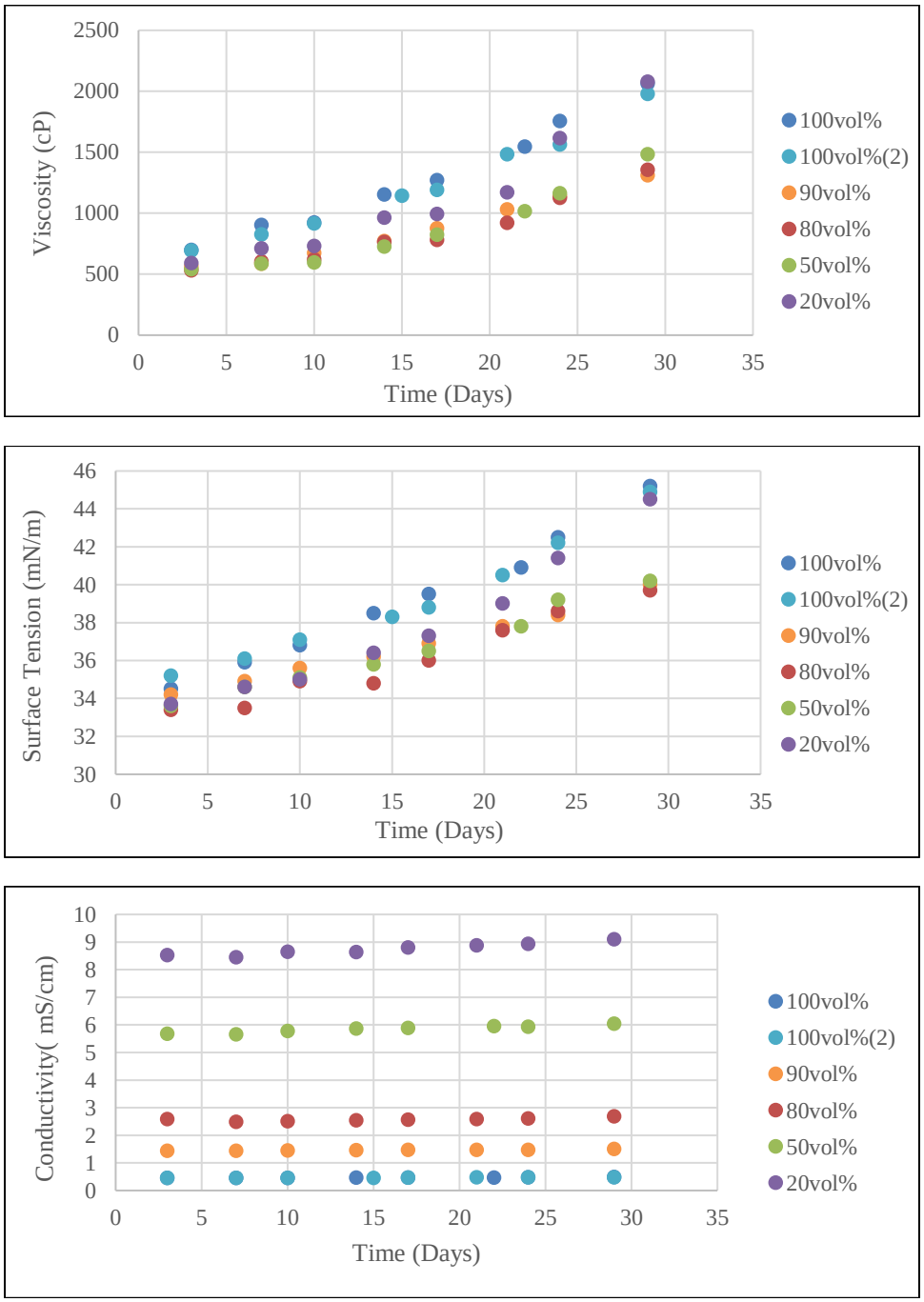

FIGURE 4: Solution property time dependence.

During electrospinning, the solutions formed a clear Taylor cone but eventually formed a gel layer on the tip of the nozzle, essentially reducing the cross-sectional area for solution flow. A droplet would form from the gel layer, which would be the site for nanofiber ejection. The optimal feed rate would be the volumetric flow at which this droplet would both grow and recede at an equal rate, allowing electrospinning for an extended time (**Figure 5**).

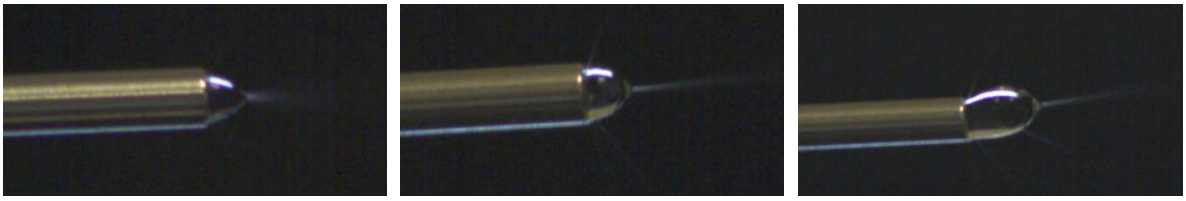

a) **b)** **c)**

FIGURE 5: The evolution of the electrospinning process from the a) Taylor cone to the b, c) gel layer.

Electrospinning feed rates decreased with increasing solution conductivity and decreasing viscosity (**Table II**). Because feed rates were approaching lower values with increasing $Al(NO_3)_3$ content and the time to build up meaningful depositions was significantly increasing, only solutions greater than 20vol% 4YSZ-Al_2O_3 were electrospun.

TABLE II: Solution Properties and Electrospinning Results

4YSZ vol%	Age (Days)	Viscosity (cP)	Surface Tension (mN/m)	Conductivity (mS/cm)	Temperature/ Humidity	Feed Rate (mL/hr)	Fiber Diameter 95% CI (nm)
100	0	699 ± 7	34.5 ± 0.14	0.463 ± 0.002	22ºC, 43%	0.5	**251 ± 31**
	11	1154 ± 13	38.5 ± 0.51	0.469 ± 0.001	23ºC, 49%	1	**292 ± 47**
	21	1755 ± 32	42.5 ± 0.31	0.482 ± 0.001	22ºC, 53%	1.62	*
100(2)	0	693 ± 5	35.2 ± 0.09	0.465 ± 0.002	23ºC, 61%	0.38	**183 ± 21**
	12	1144 ± 13	38.3 ± 0.29	0.465 ± 0.001	23ºC, 54%	0.62	**211 ± 27**
	21	1563± 7	42.2 ± 0.29	0.487 ± 0.001	23ºC, 45%	1.5	*
90	0	563 ± 8	34.2 ± 0.05	1.445 ± 0.002	23ºC, 57%	0.22	**139 ± 11**
	11	772 ± 5	36.2 ± 0.12	1.471 ± 0.001	23ºC, 56%	0.34	**193 ± 22**
	21	1140 ± 8	38.4 ± 0.17	1.481 ± 0.001	24ºC, 41%	0.4	**198 ± 24**
80	0	532 ± 10	33.4 ± 0.14	2.589 ± 0.029	23ºC, 52%	0.12	**154 ± 14**
	11	764 ± 8	34.8 ± 0.22	2.544 ± 0.003	23ºC, 52%	0.18	**123 ± 11**
	21	1125 ± 13	38.6 ± 0.22	2.612 ± 0.004	23ºC, 59%	0.27	**109 ± 8**
50	0	541 ± 9	33.6 ± 0.08	5.684 ± 0.008	23ºC, 46%	0.08	**135 ± 8**
	11	727 ± 10	35.8 ± 0.17	5.869 ± 0.007	23ºC, 43%	0.09	**184 ± 20**
	21	1163 ± 31	39.2 ± 0.56	5.938 ± 0.004	23ºC, 53%	0.1	*
20	0	592 ± 25	33.7 ± 0.16	8.533 ± 0.009	24ºC, 48%	0.05	**141 ± 12**
	11	963 ± 4	36.4 ± 0.05	8.639 ± 0.006	23ºC, 53%	0.08	*
	21	1615 ± 31	41.4 ± 0.21	8.945 ± 0.011	22ºC, 53%	0.09	*

* = did not electrospin at all

Generally, as-spun nanofiber diameter was negatively correlated with solution conductivity, and thus positively correlated with feed rate. With increasing conductivity, the greater number of ions increases molecular repulsion in solution, causing more significant stretching between emitter and collector. The nanofiber morphologies ranged between smooth and beaded, with greater bead densities in lower viscosity and more conductive membranes (**Figure 6**). Additionally, the membranes are aligned preferentially in a single direction; this is because of the rotating drum collector. A fiber will land on the collector and be wrapped around in the direction of drum rotation.

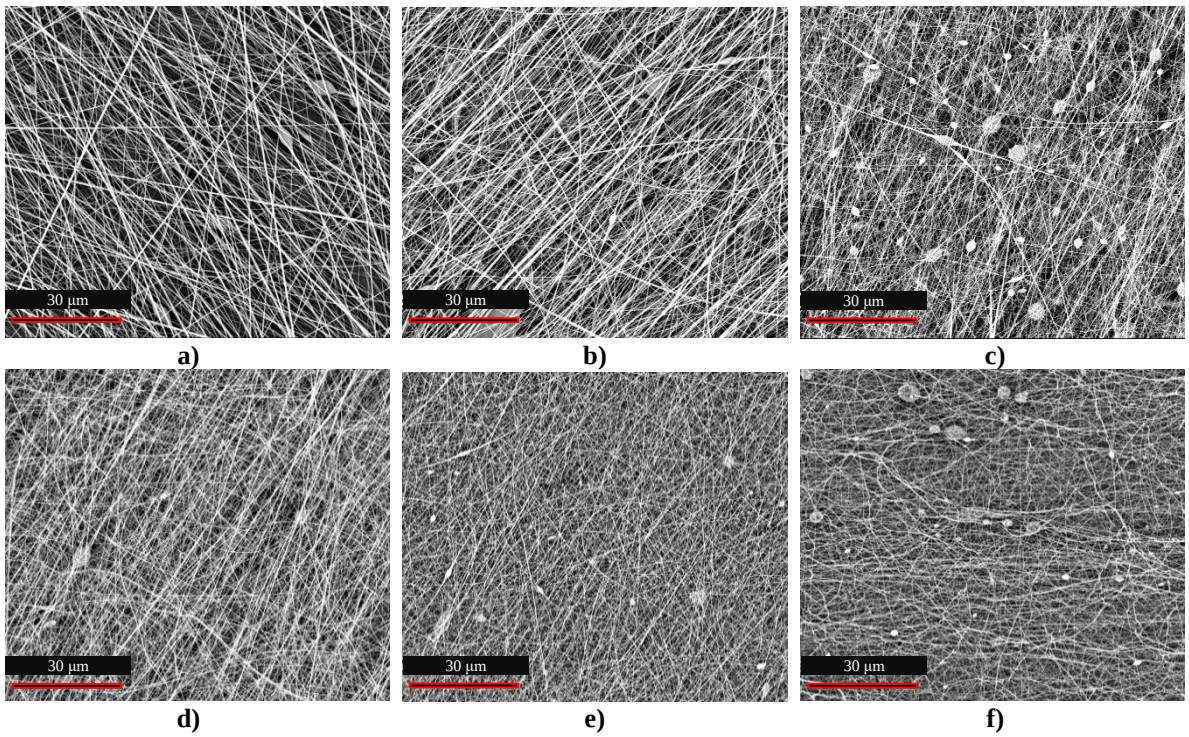

FIGURE 6: Initially electrospun nanofiber membranes spun from a, b) 100vol%, c) 90vol%, d) 80vol%, e) 50vol%, and f) 20vol% 4YSZ-Al_2O_3 solutions.

The aged solutions did not spin well once viscosity exceeded 1000 cP. More viscous solutions resist fiber stretching, feature thicker jets, and require higher feed rates to maintain a stable process, leading to an increase in fiber diameters and electrosprayed droplets in the mat. The concentration of droplets in the nanofiber membranes significantly increased in the aged solutions. The 80vol% 4YSZ-Al_2O_3 membranes featured increasing droplet concentrations with age (**Figure 7**). Additional microstructures for all compositions are in **Appendix A-1**.

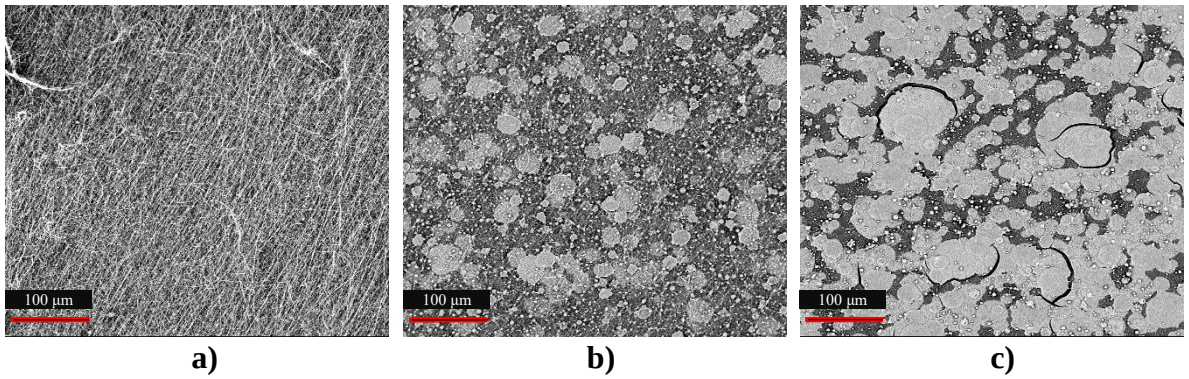

FIGURE 7: Morphology of electrospun 80vol% 4YSZ-Al_2O_3 nanofiber membranes after a) initial solution mixing, b) solution aging for 11 days, and c) solution aging for 21 days.

Because the aged solutions tended to electrospin and electrospray droplets into the nanofiber membranes, only the initially electrospun membranes were calcined. Additionally, the 50 and 20vol% 4YSZ-Al_2O_3 fibers were unable to be peeled, so the ceramics were not fibrous, but rather powdered. The resulting 100, 90, and 80vol% 4YSZ-Al_2O_3 ceramic nanofibers were thin but robust, lending flexural strength during handling (**Figure 8**).

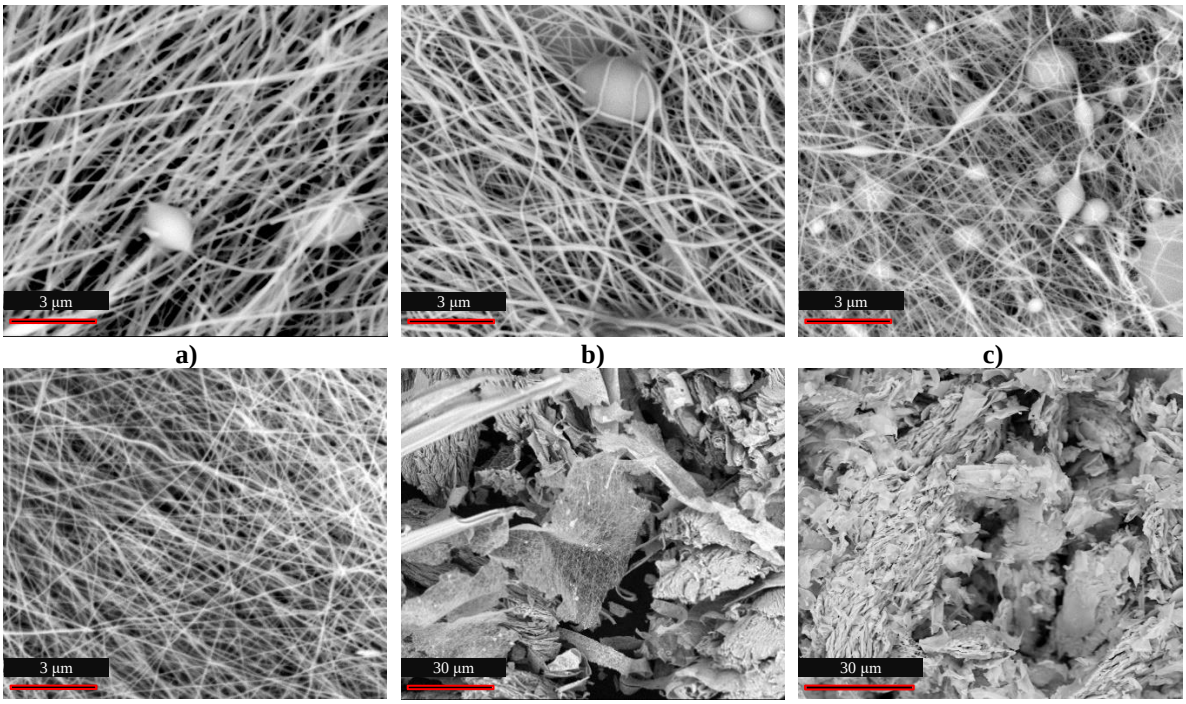

FIGURE 8: Electrospun ceramic nanofibers of a, b) 100vol% 4YSZ, c) 90vol%, d) 80vol%, e) 50vol%, and f) 20vol% 4YSZ-Al_2O_3 composites.

The EDX spectra (see **Appendix A-2**) indicate an overestimation of oxygen content and subsequent incorrect Zr:Y ratios. The EDX spectra give relative 4YSZ:Al_2O_3 volume compositions of 1, 1, 0.87, 0.74, 0.45, and 0.17 with increasing $Al(NO_3)_3$ content (**Table III**). This is not significantly different from the target 4YSZ:Al_2O_3 volume compositions of 1, 1, 0.9, 0.8, 0.5, and 0.2, where the difference could arise from the overestimation of oxygen content. The post-electrospinning annealed nanofiber diameters are a function of the precursor content in solution rather than the initial as-spun fiber diameters, decreasing with alumina content.[13]

TABLE III: Ceramic Nanofiber Morphological Characteristics

Expected 4YSZ vol%	Zr wt%	Y wt%	Al wt%	O wt%	Zr:Y Molar Ratio	Actual YSZ vol%	Fiber Diameter 95% CI (nm)
100	50.63	7.01	0	42.36	7.04	100	**93.7 ± 0.3**
100(2)	53.79	7.22	0	38.99	7.26	100	**91.0 ± 0.4**
90	43.44	5.67	3.51	46.88	7.47	87	**62.9 ± 0.6**
80	38.17	4.92	6.87	50.04	7.56	74	**56.6 ± 0.3**
50	27.82	3.59	18.02	50.57	7.55	45	*
20	17.18	1.44	41.75	31.25	11.63	17	*

* = ceramic nanofibers not observed

DISCUSSION

The precursor solutions experienced aging effects, mainly in the form of viscosity and surface tension increases that were only reversed after extensive shearing at high shear rates. Because viscosity and surface tension resist jet formation and jet stretching, electrospinning does not occur as easily with solution age. The precursors, zirconium acetate and aluminum nitrate, require investigation to determine which is responsible for the variable solution properties and PVP crosslinking. Zirconium acetate has been used as a complexing agent for polymers containing

carboxylate [COO^-] functional groups, where gelation rate is dependent on crosslinker concentration and salinity, or ionic concentration.[32] The PVP monomer, N-vinylpyrrolidone, does not contain a carboxylate group, but consists of a cyclic amide, known as a lactam, linked to an alkane backbone. The carbonyl [C=O] group in the cyclic amide has a lone pair of electrons that are easily available for intermolecular hydrogen bonding. The carbonyl group is in resonance with the nitrogen, meaning the bond is delocalized between an electronegative oxygen and a positively charged nitrogen (**Figure 10a**). This [$-N^+=C-O^-$] resonance structure, to which positive cations like Al^{3+} and Zr^{4+} or hydrogen ions can attach through coordinative bonding,[33, 34] is preferred in polar solvents, such as water and ethanol, compared to its neutral structure.[35] Aqueous zirconium(IV) can form different complexes in solution through hydrolysis and polymerization. During hydrolysis, or reaction with water, a tetranuclear complex $[Zr_4(OH)_8(H_2O)_{16}]^{8+}$ develops from 8 hydroxyl $[OH]^-$ groups bridging between a square Zr^{4+} core.[36, 37] In the presence of acetic acid, aqueous zirconium acetate will form a zirconium hydroxyl-bridged polymer with coordinated water and acetoxy functional groups attached (**Figure 10b**).[38] The readily available hydroxyl groups formed through deprotonation of coordinated water facilitates strong hydrogen bonding and electrostatic forces between the PVP and zirconium complex side groups (**Figure 10c)**.[5, 38] The positively charged nitrogen can form intermolecular attractions with negatively charged, disassociated ions. This explains why the pure 4YSZ solution, with the greatest concentration of zirconium acetate crosslinker, and the solution with the greatest $Al(NO_3)_3$ concentration experienced the greatest increase in viscosity. However, zirconium acetate needs to be present to facilitate gelation; a solution with purely PVP, water, ethanol, and $Al(NO_3)_3$ did not gel after 2 months. Further investigation such as UV-vis and Fourier-transform infrared (FTIR) spectroscopy is warranted to confirm the proposed mechanism. Different aluminum precursors, such as aluminum acetate, should also be investigated for extending solution shelf-life.

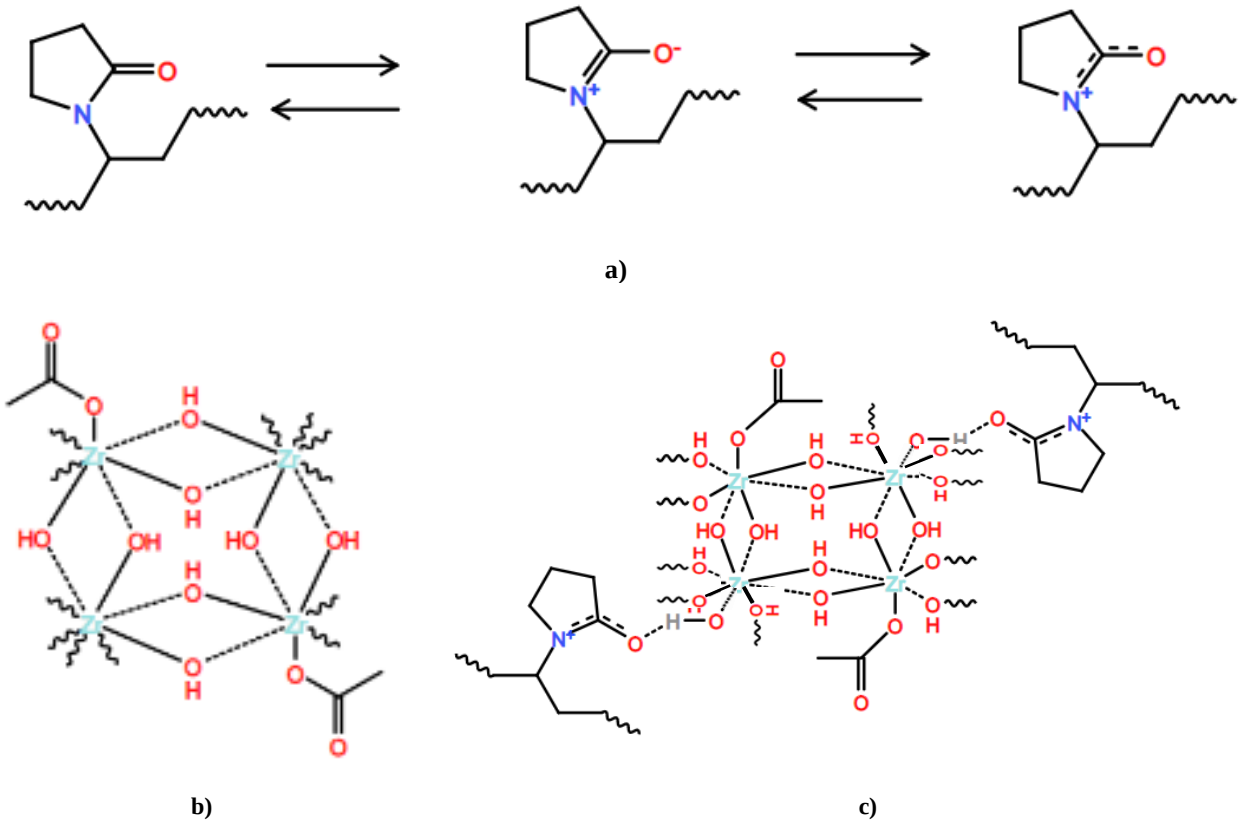

FIGURE 10: The reaction between the a) PVP resonance structure and b) polymerized zirconium acetate hydrate complex as a c) possible mechanism to crosslinking intermolecular hydrogen bonding. The introduction of negative ions (i.e. nitrates) will lead to additional intermolecular forces at positive nitrogen sites on the PVP monomer.

Electrospinning feed rate can be described in terms of a solution's properties. Often, the feed rate (Q) is described in terms of a power law relationship with jet current (I) when voltage is kept constant.[39] In literature, jet current is often measured by having an ohmic resistor in series with the collector and ground.[40, 41] In order to better predict feed rate from solution properties, a parameter involving viscosity, surface tension, and conductivity is constructed (**Figure 11**). A power law relationship, with R^2 = 0.95, is observed between feed rate and the "inductance parameter" [$\eta(\sigma\gamma)^{-1}$], labeled as such due to having the same units, [J/A^2], as electromagnetic inductance. The relationship should only hold true for solutions spun across a constant electric field strength and with a given experimental setup (i.e. emitter size, emitter type).

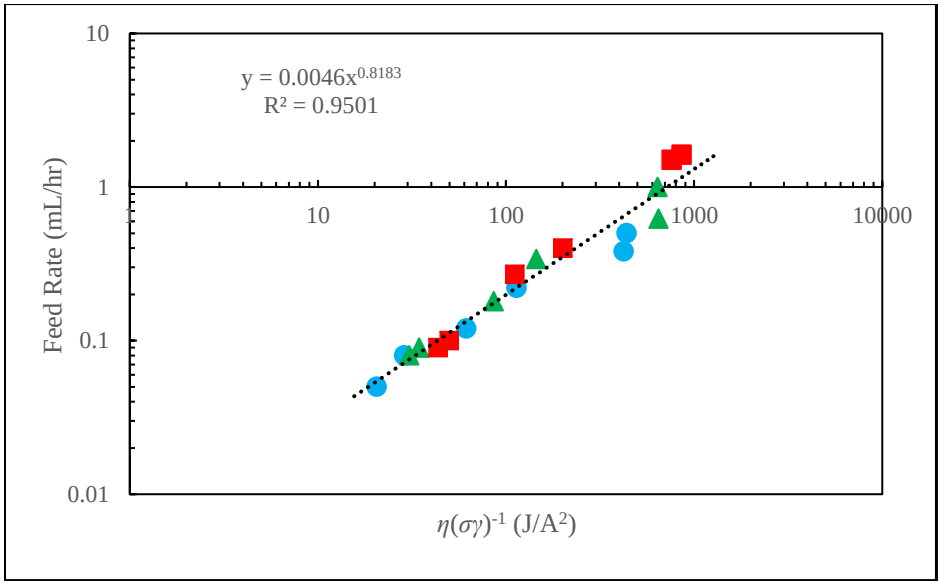

FIGURE 11: Power law relationship between solution feed rate and the solution property "inductance parameter", $\eta(\sigma\gamma)^{-1}$, where circles are initial electrospinning, triangles are electrospinning after 1st aging, and squares are electrospinning after 2nd aging.

Beading typically arises from solutions with low viscosities,[12] such as the 90vol% 4YSZ-Al_2O_3, which had the lowest initial viscosity and highest density of beads. Nanofiber beading in membranes could also suggest an unoptimized feed rate; if the feed rate were too high, excess solution gathered at the emitter could be carried away with ejected material, causing variable jet thicknesses and differential fiber stretching due to insufficient solvent evaporation for large droplets compared to jets. This is entirely possible when considering the extremely low feed rates used for the 20vol% 4YSZ-Al_2O_3. The optimal feed rates were reaching the limits of the instrument's sensitivity and capability, and any deviation from the low feed rate could introduce microstructural defects. This implies a conductivity limit for meaningful and controlled nanofiber deposition; for the experimental electrospinning setup described here, a conductivity between 2 and 5 mS/cm hinders electrospinning, which is in agreement with literature.[42]

Additionally, excessive feed rates can affect the average size and spread of nanofiber diameter size distributions. Thicker jets and jet splitting can occur on large droplets collected at the emitter, leading to greater and more variable fiber size distributions.[43] This can be seen from the nanofiber morphologies of the two 100vol% 4YSZ solutions, where the solution spun at higher feed rates had a greater average fiber diameter with much more variability. Droplets seemed to be a consequence of high viscosities; a limit between 700 and 1100 cP is established as an electrospinning limit depending on conductivity. Droplets and beading in the mat may also contribute to more spread in fiber size distribution. A jet of variable thickness will experience variable stretching, where the acceleration of conductive material in an electric field is dependent on the charge and inversely proportional to particle mass. Compared to a free jet, which will accelerate significantly according to its small radius, a jet that is constrained between slow moving droplets should experience additional time for solvent evaporation and, subsequently, additional stretching. This mechanism could explain why membranes with higher density of fiber beading featured smaller fiber diameters.

As-spun fiber diameter is correlated with electrospinning parameters and solution properties. In the yttria-alumina-zirconia system, increasing conductivities and decreasing feed rates are accompanied by a decrease in fiber diameter, while longer aging times and increasing feed rates are accompanied by an increase in fiber diameter and microstructural defects. Sigmund *et al.*[43] has correlated fiber diameter (h) with feed rate, surface tension, and current carried by the nanofiber jet with the use of a constant, c (**Equation 2**). Jet current can be rewritten in terms of conductivity, electric field strength (E), and feed rate (**Equation 3**).[39]

$$h \sim c\left(\frac{Q}{I}\right)^{2/3}\gamma^{1/3} \tag{2}$$

$$I = EQ^{0.5}\sigma^{0.4} \tag{3}$$

The fiber diameters observed in the yttria-alumina-zirconia can be predicted as a function of solution properties and electrospinning parameters. Substituting **Equation 3** into **Equation 2** yields a poorly predictive linear relationship between fiber diameter and $[Q^{0.5}(\sigma^{0.4}E)^{-1}]^{2/3}\,\gamma^{1/3}$, with an $R^2 = 0.66$. This is because the assumption for jet current does not account for solution viscosity. Additionally, jet current may not be related linearly to electric field strength.[41] A parabolic trendline yields an $R^2 = 0.74$ (**Figure 12**). Further measurement of jet current should yield a more predictive relationship between fiber diameters and process parameters and provide a more systematic approach to optimizing feed rates.

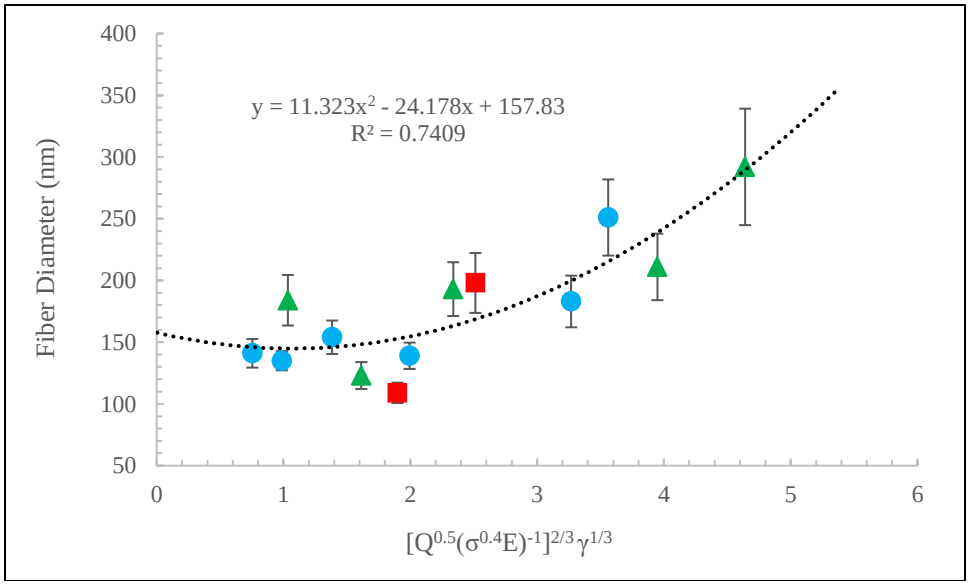

FIGURE 12: Relationship between as-spun nanofiber diameter and electrospinning variables, where circles are initial electrospinning, triangles are electrospinning after 1st aging, and squares are electrospinning after 2nd aging.

The calcined fiber diameters appear independent of as-spun fiber diameters. Ceramic fiber diameter decreased as 4YSZ composition decreased. Because alumina is added to stabilized zirconia as a sintering inhibitor,[27] the fiber diameter and crystallite size should be reduced with increasing alumina content. Based on the characterization presented, the 80vol% 4YSZ-Al_2O_3 fibers should be pursued for further investigation due to its slow aging kinetics, small fiber diameter, lack of embrittling droplets and beads, and ability to be electrospun with age. Further heat treatment optimization through thermogravimetric analysis (TGA) and X-ray diffraction (XRD) should be performed to determine the present crystal structures in the microstructure at different annealing temperatures.

CONCLUSIONS

Novel yttria-alumina-zirconia nanofibers can be electrospun with average fiber diameters less than 300 nm from precursor solutions consisting of zirconium acetate in acetic acid, aluminum/yttrium nitrates, and PVP.

1. There is an aging effect, revealed by time-dependent solution viscosity and surface tension increases, associated with strong hydrogen bonding between hydrated zirconium acetate complexes and PVP functional groups, as well as intermolecular interactions between disassociated ionic species. The proposed gelation mechanism is driven by zirconium acetate concentration and can only be reversed through extensive shearing at high shear rates.

2. Generally, solution conductivity is negatively correlated with feed rate, while solution viscosity is positively correlated. Feed rates can be extrapolated in terms of solution properties, $\eta(\sigma\gamma)^{-1}$, for a given experimental setup and electric field strength. The upper limit for successful electrospinning were established to be between 2 and 5 mS/cm, and 700 and 1100 cP for solution conductivity and viscosity, respectively.

3. The ceramic nanofibers formed through annealing at 1000ºC for 2 hours were amorphous and between 50 and 100 nm in diameter. The 4YSZ-Al_2O_3 nanofiber diameter was dependent on alumina volume rather than original electrospun diameter, therefore, the alumina ceramic phase successfully hindered stabilized zirconia coarsening, a promising result for stronger and tougher nanofiber production.

4. The 80vol% 4YSZ-Al_2O_3 is recommended for further investigation based on its electrospinnability across different ages, the small as-spun fiber diameter of 100 to 150 nm, the small annealed fiber diameter of 50 nm, and the lack of large and catastrophic microstructural defects.

Future work should be done to investigate the aging mechanism in the precursor and polymer interactions. Proposed experimentation includes pH monitoring over time, UV-vis and FTIR spectroscopy, and inclusion of different precursor salts. Jet current measurements should be taken to verify the relationship between fiber diameter and process parameters. X-ray diffraction should be employed in conjunction with thermogravimetric analysis to determine the optimal annealing temperature to produce a microstructure for optimal fracture toughness.

ACKNOWLEDGEMENTS

Financial support for ceramic nanofiber research and development at Lawrence Livermore National Laboratory has been provided by the Nuclear Safety Research and Development Program for the Department of Energy (NSRD-12, NSRD-20) and NNSA Nuclear Safety Research and Development (NSR&D) Program. Additionally, the authors would like to acknowledge advice and support provided by Mark Mitchell, Nick Teslich, Dennis Luong, Wayne Jensen, Dwight Squires, Chantel Aracne-Ruddle, Danny Laycak, and Howard Wong.

The authors would also like to thank the Summer Undergraduate Laboratory Internship (SULI) for the opportunity to advance their experience in the materials science field at a Department of Energy national laboratory, as well as for the opportunity to network with many mentors and experts in their respective fields, including the members of the Polymers and Ceramics Group.

APPENDIX

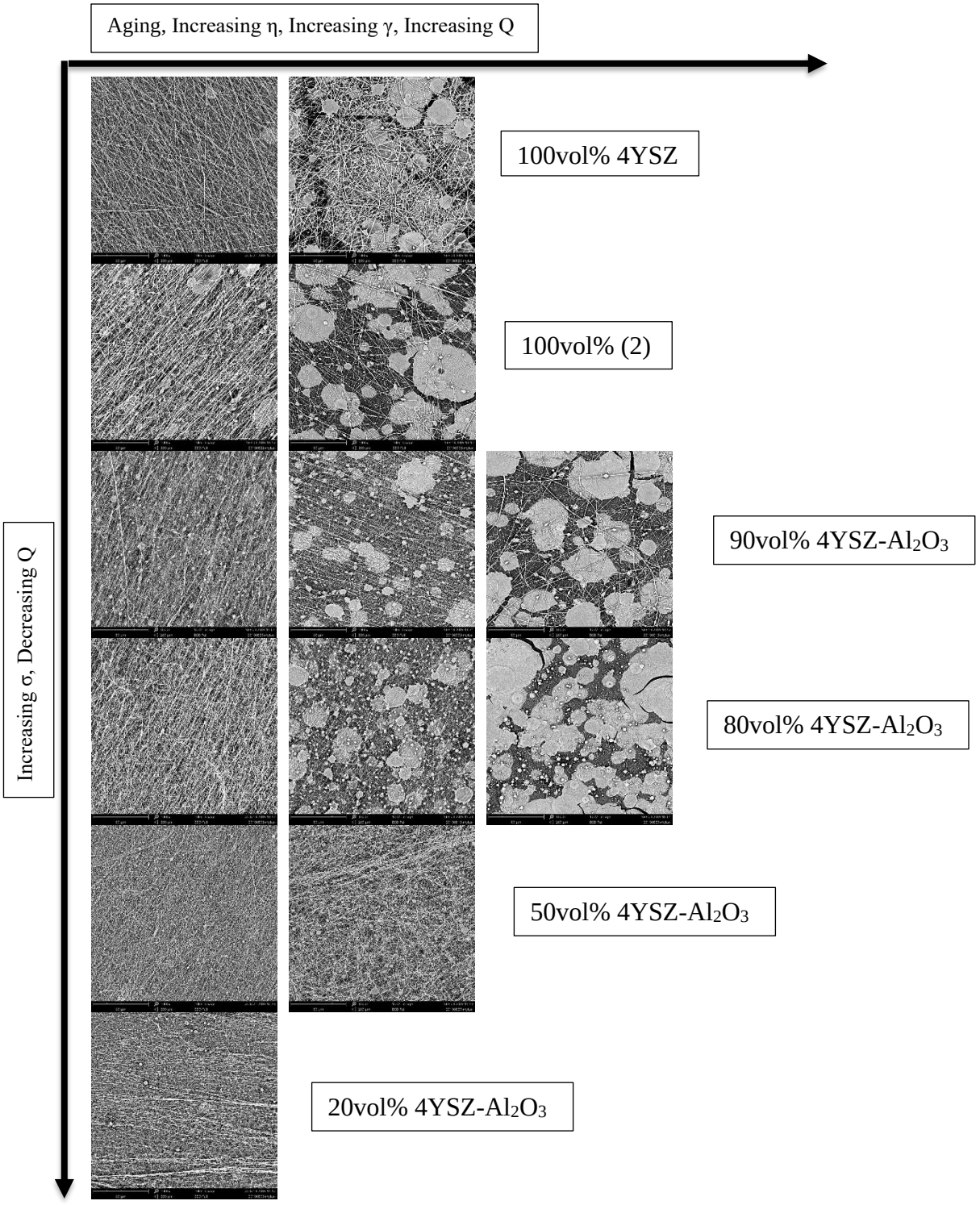

A-1: Microstructural and parameter space evolution of aged solutions with different concentrations of $Al(NO_3)_3$ at 1000x magnification.

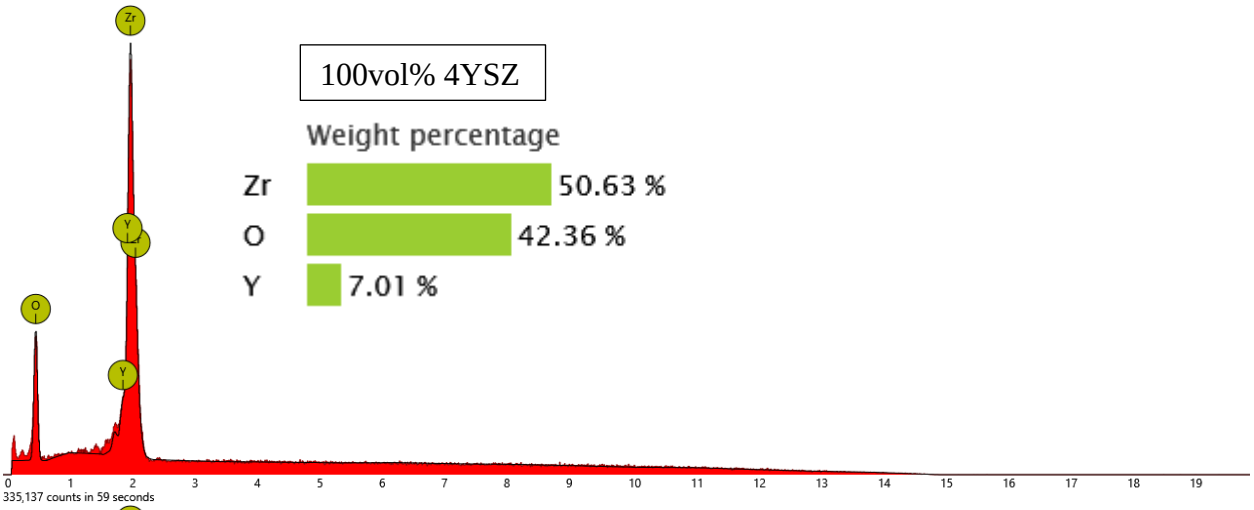
100vol% 4YSZ
Weight percentage
Zr 50.63 %
O 42.36 %
Y 7.01 %
335,137 counts in 59 seconds

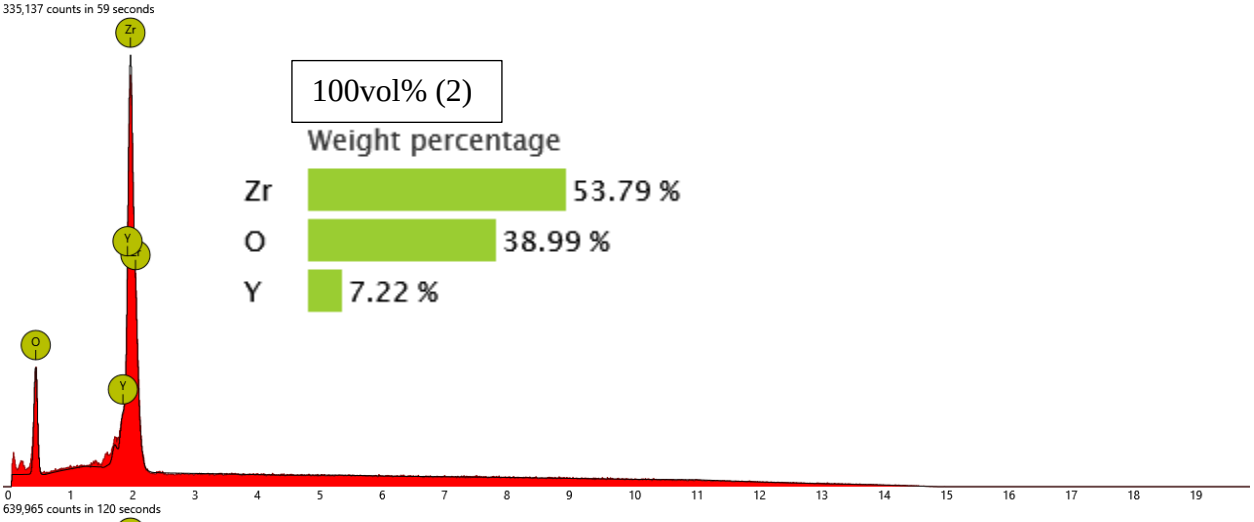
100vol% (2)
Weight percentage
Zr 53.79 %
O 38.99 %
Y 7.22 %
639,965 counts in 120 seconds

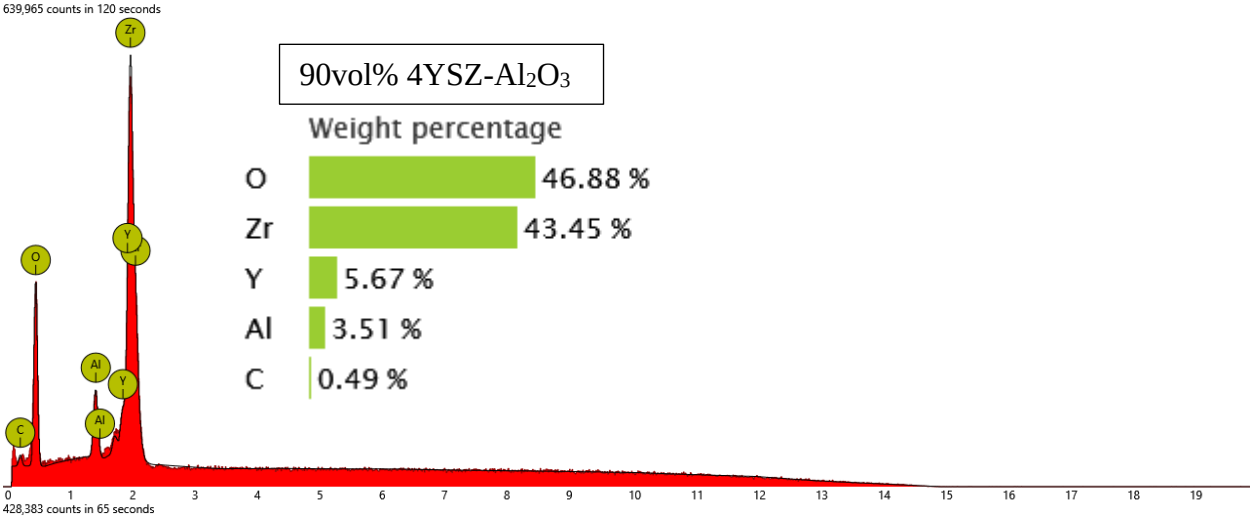
90vol% 4YSZ-Al2O3
Weight percentage
O 46.88 %
Zr 43.45 %
Y 5.67 %
Al 3.51 %
C 0.49 %
428,383 counts in 65 seconds

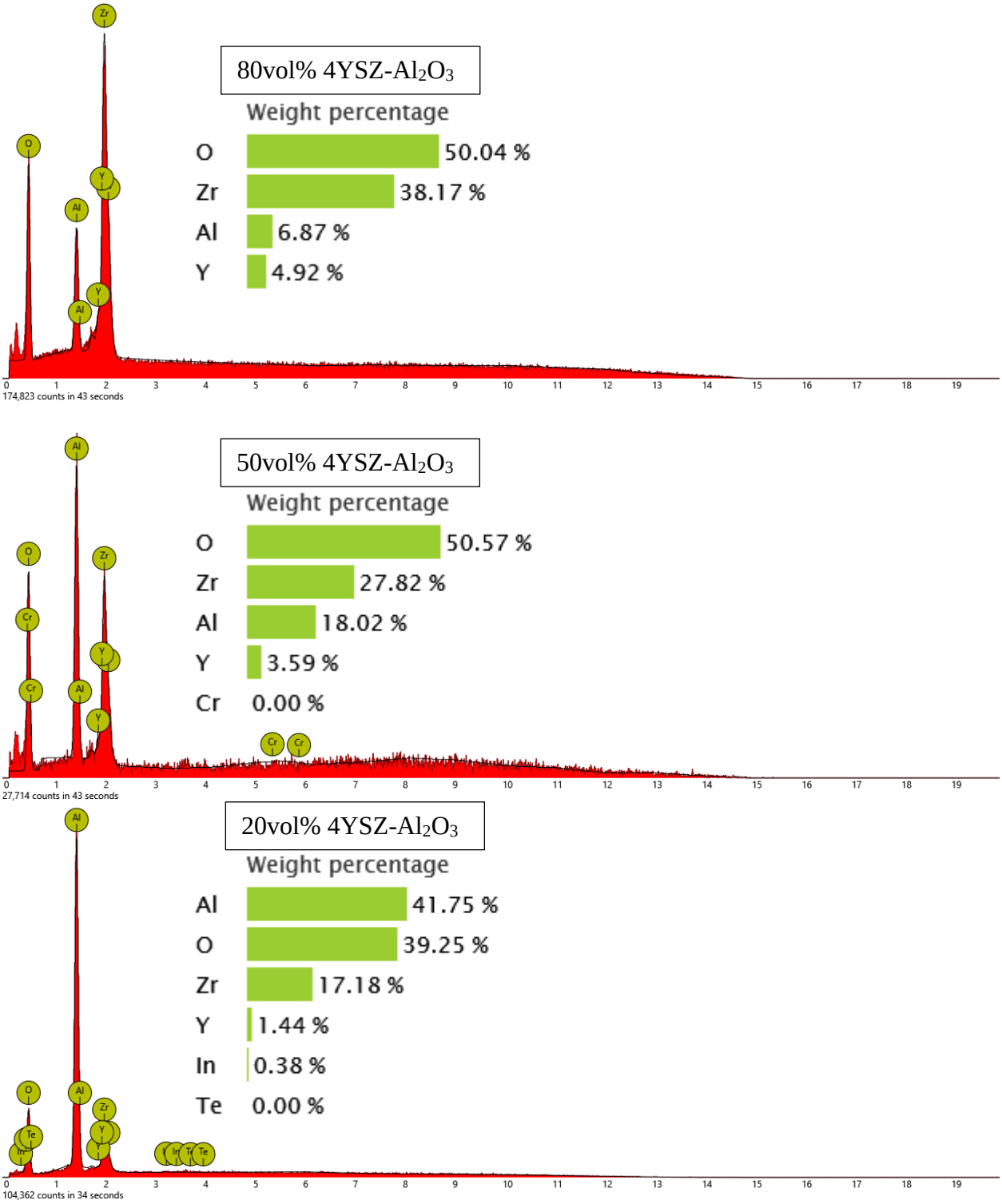

A-2: EDX spectra for 4YSZ-Al_2O_3 ceramic nanofibers with compositions of 100, 90, 80, 50, and 20 volume fraction 4YSZ.

REFERENCES

1. K. Katsogiannis, G. Vladisavljević and S. Georgiadou, *European Polymer Journal* **69**, 284-295 (2015).
2. S. Janjanin, W. Li, M. Morgan, R. Shanti and R. Tuan, *Journal of Surgical Research* **149**, 47-56 (2008).
3. S. Wen, M. Liang, R. Zou, Z. Wang, D. Yue and L. Liu, *RSC Advances* **5**, 41513-41519 (2015).
4. W. Ma, Y. Xu, K. Ma and H. Zhang, *Applied Catalysis A: General* **526**, 147-154 (2016).
5. X. Mao, Y. Bai, J. Yu and B. Ding, *J. Am. Ceram. Soc.* **99**, 2760-2768 (2016).
6. X. Song, Z. Liu and D. Sun, *Advanced Materials* **23**, 3256-3260 (2011).
7. C. Martin, *Accounts of Chemical Research* **28**, 61-68 (1995).
8. C. Zhang, X. Xue, Q. Luo, Y. Li, K. Yang, X. Zhuang, Y. Jiang, J. Zhang, J. Liu, G. Zou and X. Liang, *ACS Nano* **8**, 11715-11723 (2014).
9. D. Li and Y. Xia, *Advanced Materials* **16**, 1151-1170 (2004).
10. B. Cramariuc, R. Cramariuc, R. Scarlet, L. Manea, I. Lupu and O. Cramariuc, *Journal of Electrostatics* **71**, 189-198 (2013).
11. R. Stepanyan, A. Subbotin, L. Cuperus, P. Boonen, M. Dorschu, F. Oosterlinck and M. Bulters, *Polymer* **97**, 428-439 (2016).
12. G. Cadafalch Gazquez, V. Smulders, S. Veldhuis, P. Wieringa, L. Moroni, B. Boukamp and J. ten Elshof, *Nanomaterials* **7**, (2017).
13. J. Koo, S. Hwang, M. Ahn, M. Choi, D. Byun and W. Lee, *J. Am. Ceram. Soc.* **99**, 3146-3150 (2016).
14. E. Orowan, *Reports on Progress in Physics* **12**, 185-232 (1949).
15. Y. Zhu, W. Blumenthal, S. Taylor, T. Lowe and B. Zhou, *J. Am. Ceram. Soc.* **80**, 1447-1452 (2005).
16. R. Garvie, R. Hannink and R. Pascoe, *Nature* **258**, 703-704 (1975).
17. F. Lange, *J. Mater. Sci.* **17**, 225-234 (1982).
18. N. Claussen, *J. Am. Ceram. Soc.* **59**, 49-51 (1976).
19. N. Claussen, J. Steeb and R. F. Pabst, *Am. Ceram. Soc. Bull.* **55,** 559 (1977).
20. Y. Fu and A. Evans, *Acta Metallurgica* **33**, 1515-1523 (1985).
21. A. Evans and K. Faber, *J. Am. Ceram. Soc.* **64**, 394-398 (1981).
22. N. Claussen, *J. Am. Ceram. Soc.* **61**, 85-86 (1978).
23. J. Wang and R. Stevens, *J. Mater. Sci.* **23**, 804-808 (1988).
24. P. Becher, *Acta Metallurgica* **34**, 1885-1891 (1986).
25. M. Rühle, A. Evans, R. McMeeking, P. Charalambides and J. Hutchinson, *Acta Metallurgica* **35**, 2701-2710 (1987).
26. J. Wang, PhD Thesis, Department of Ceramics, University of Leeds (1986).
27. R. Garcia, V. Ussui, N. de Lima, E. Muccillo and D. Lazar, *J. Alloys Compd.* **486**, 747-753 (2009).
28. K. Dychtoń, M. Drajewicz, M. Pytel, P. Rokicki and A. Nowotnik, *J. Therm. Anal. Calorim.* **126**, 1-7 (2016).
29. V. Rodaev, A. Zhigachev and Y. Golovin, *Ceramics International* **43**, 16023-16026 (2017).
30. İ. Uslu, T. Tunç, S. Keskin and M. Öztürk, *Fibers and Polymers* **12**, 303-309 (2011).
31. C.A. Schneider, W.S. Rasband, and K.W. Eliceiri, *Nature Methods* **9**, 671-675 (2012).
32. C. Dai, G. Zhao, Q. You and M. Zhao, *Journal of Applied Polymer Science* **131**, (2013).
33. S. Gottapu, S. Padhi, M. Krishna and K. Muralidharan, *New Journal of Chemistry* **39**, 5203-5207 (2015).
34. A. Keiteb, E. Saion, A. Zakaria and N. Soltani, *J. of Nanomaterials* **2016**, 1-6 (2016).
35. J. Wang, T. Tsuzuki, B. Tang, P. Cizek, L. Sun and X. Wang, *Colloid Polym. Sci.* **288**, 1705-1711 (2010).
36. V. Kanazhevskii, B. Novgorodov, V. Shmachkova, N. Kotsarenko, V. Kriventsov and D. Kochubey, *Mendeleev Communications* **11**, 211-212 (2001).
37. C. Hennig, S. Weiss, W. Kraus, J. Kretzschmar and A. Scheinost, *Inorganic Chemistry* **56**, 2473-2480 (2017).
38. G. Sun, F. Liu, J. Bi and C. Wang, *J. Alloys Compd.* **649**, 788-792 (2015).
39. S. Theron, E. Zussman and A. Yarin, *Polymer* **45**, 2017-2030 (2004).
40. D. Fallahi, M. Rafizadeh, N. Mohammadi and B. Vahidi, *E-Polymers* **9**, (2009).
41. F. Yalçinkaya, *Tekstil ve Konfeksiyon* **25**, 202-206 (2015).
42. B. De Schoenmaker, A. Goethals, L. Van der Schueren, H. Rahier and K. De Clerck, *J. Mater. Sci.* **47**, 4118-4126 (2012).
43. F. Abdel-Hady, A. Alzahrany and M. Hamed, *ISRN Nanotechnology* **2011**, 1-14 (2011).
44. W. Sigmund, J. Yuh, H. Park, V. Maneeratana, G. Pyrgiotakis, A. Daga, J. Taylor and J. Nino, *J. Amer. Ceram. Soc.* **89**, 395-407 (2006).